

Comparison of tissue characterization curves for different CT scanners: implication in proton therapy treatment planning

Chee-Wai Cheng^{1,2}, Li Zhao^{1,2}, Mark Wolanski^{1,2}, Qingya Zhao^{1,3}, Josuha James⁴, Kate Dikeman⁴, Michael Mills⁴, Mei Li⁵, Shiv P. Srivastava⁶, Xing Qi Lu⁷, Indra J. Das^{1,2}

¹Indiana University Health Proton Therapy Center, Bloomington, IN, 47408, USA; ²Department of Radiation Oncology, Indiana University School of Medicine, Indianapolis, IN, 46202, USA; ³Department of Radiation Oncology, Parkview Health, Fort Wayne, IN, USA; ⁴Department of Radiation Oncology, University of Louisville, Louisville, KY, 40202, USA; ⁵Department of Radiation Oncology, Morristown Memorial Hospital, Morristown, NJ, 07962, USA; ⁶Purdue University, West Lafayette, and Reid Hospital, Richmond, IN, 47374, USA; ⁷Beth Israel Deaconess Medical Center, Harvard Medical School, Boston, MA 02215, USA

Corresponding to: Chee-Wai Cheng, Ph.D. Indiana University Health Proton Therapy Center, Bloomington, IN, 47401, USA. Email: ccheng1@iuhealth.org.

Abstract: For proton beam therapy, CT imaging is required to calculate dose based on CT pixel values of relative stopping power (RSP). The variation among CT-scanners and the phantom used to derive the relationship CT number-electron density-RSP has not been investigated. Using RMI CT phantoms, 18 CT scanners and a Tomotherapy unit, the Hounsfield unit (HU) variations and associated dosimetric uncertainty were investigated. The variation of HU was within one standard deviation (SD) of the average for 14 out of the 15 scanners tested with the same phantoms. For high density materials (>400 HU) the HU values deviated by more than 4% from the average. The HU-RSP curves of 18 scanners were fitted with a straight line in three HU intervals: $-700 < \text{HU} < 0$, $0 < \text{HU} < 230$ and $230 < \text{HU} < 1,700$. The dosimetric impacts of the variation of HU among scanners were <1% in DVH point dose comparisons in a prostate cancer plan. For a head and neck cancer plan the difference was up to 4% due to large inhomogeneities. Our results seem to suggest that the X-ray spectrum of a CT scanner has a smaller effect on the HU-RSP curve than the elemental compositions of the tissue substitutes used in the calibration. Furthermore, a single HU-RSP curve may suffice as a reference curve for proton treatment planning. It is found to agree with the calibration curve obtained for the specific scanner. This study does not address the issue of metallic implants included in the treatment plan.

Key Words: Proton beam; CT scanner; electron density; relative stopping power; dosimetric uncertainty



Submitted Oct 25, 2012. Accepted for publication Nov 30, 2012.

doi: 10.3978/j.issn.2218-676X.2012.11.05

Scan to your mobile device or view this article at: <http://www.thetcr.org/article/view/811/html>

Introduction

In modern radiation therapy, CT is used to provide the anatomical information of the targets and organs at risk (OAR) for treatment planning of a patient. To determine the dose deposited in each pixel of a CT data set, the relative electron density (RED) must be known a priori. This is enabled by a tissue characterization curve (TCC) that assigns the Hounsfield unit (HU) of each pixel to an associated RED value. Conventionally, the TCC for a given kVp of a CT scanner is generated from a calibration measurement using

a tissue characterization phantom. A commonly used tissue characterization phantom is the RMI 467 (Gammex Inc., Middleton, WI) that contains a number of tissue substitutes made in the form of cylindrical rods 2.8 cm in diameter arranged in two concentric circles in a 33 cm diameter solid water phantom slab. Each tissue substitute rod has a specific elemental composition (considered as confidential information by the vendor) to reproduce the physical characteristics of the tissue it represents (for example, electron density and physical density). The HU of each tissue

substitute material averaged over a certain region-of-interest (ROI) is obtained from the CT scan. A plot of the HU of the tissue substitutes versus their corresponding RED values (supplied by the manufacturer) produces the TCC for that particular kVp for a given CT scanner.

Variations in CT numbers among different diagnostic scanners for the same materials and their locations and orientations inside the scanner were reported more than 30 years ago (1,2). With the emergence of three dimensional treatment planning in the 1990s, CT-based treatment planning became the standard of practice in radiation therapy. Subsequently, the use of TCC in treatment planning has become a norm as reported by many investigators (3-7). Thomas (7) studied TCC for a number of CT scanners and reported that using a single table for all the scanners would produce dosimetric errors of <0.8% for 6 MV X-rays. It was also reported that a 1% error in dosimetry would require errors over 8% in the bone electron density in external beam radiation therapy (7). Kilby *et al.* (6) found that a greater precision in electron density is required as the photon beam energy decreases or the tissue thickness increases. For 6 MV photons, the reported tolerance level of electron densities from Kilby *et al.* (6) are in agreement with those reported earlier by Thomas (7). However, tissue substitute materials may not accurately mimic the radiation characteristics of the real tissues due to the differences in the elemental compositions. Schneider *et al.* (8) pointed out that there is a strong dependence of the TCC on the choice of the tissue substitute materials as photon attenuation in a CT scanner depends not only on the Compton scattering, but also on the photoelectric effect and coherent scattering. A stoichiometric method to generate a more accurate TCC was proposed using both the measured HU and the chemical composition of real tissues (8). As HU is the ratio of the attenuation coefficient of a material to that of water, the value is affected by the beam hardening effect. Schneider *et al.* (8) suggested that all tissue substitute materials should be scanned at the center of the CT scanner so that each material is irradiated by the same X-ray spectrum.

For treatment planning in proton beam therapy (PBT), RED must be first converted to the corresponding relative stopping power (RSP) values. This is done using the Bethe-Bloch equation as shown by Bichsel (9):

$$RSP = \rho_e^{rel} \{ \ln(2m_0c^2\beta^2/[I_t(1-\beta^2)] - \beta^2) / \{ \ln(2m_0c^2\beta^2/[I_w(1-\beta^2)] - \beta^2) \} \} \quad [1],$$

where ρ_e^{rel} is the RED of the material, I_t is the ionization potential of the material, m_0 is the electron rest mass, c is

the speed of light and β is the ratio v/c , v being the speed of proton.

The effect of the elemental composition of tissue substitutes on the TCC is more pronounced in PBT due to the energy dependence of the proton range and the stopping powers in tissue, which in turn depends on the elemental composition of the tissues. Yohannes *et al.* (10) proposed a semi-empirical model in the stoichiometric calibration based on which a new formulation of tissue substitute materials was proposed (11). These new tissue substitute materials closely resemble the radiation and physical characteristics of those of the standard real tissues in ICRU Report 44 (12) and allow the generation of an accurate TCC efficiently. The accuracy of the stoichiometric calibration has been verified in proton beam (13). On the other hand, Qi *et al.* (14) found that the CT scan technique (kilo-voltage) and the patient support table top have the most impact on the HU, whereas changing the positions of the tissue substitute rods in the RMI phantom resulted in <1% change in HU for lung and cortical bone.

With advancements in CT technology in recent years, CT scanners used in radiation oncology are mostly multi-slice high resolution scanners and some are equipped with dose and artifact reduction capabilities. A question arises: could modern technology reduce the inconsistencies in HU among the different CT scanners that have been observed earlier (1,2,7)? In other words, how different are the TCC among the different modern scanners in the radiotherapy clinics, giving the same model of the tissue characterization phantom? Alternatively, do all CT scanners produce identical TCC using the same tissue characterization phantom? Ultimately, the question we want to answer is: what is the dosimetric implication in PBT due to differences in TCC?

In this study, we have carried out a systematic study to examine the HU-RSP curves obtained from a wide array of CT scanners and to investigate the effects of the differences in HU-RSP curves on dose distributions in PBT. This study did not include CT scans containing metallic structures such as implants.

Methods

Comparison of HU variation in different RMI phantoms

Using the RMI 467 phantom, HU-RED curves were obtained from 18 different CT scanners in nine institutions for 120 kVp (mAs was not a controlled experimental variable and may have been different for different institutions). In addition, a HU-RED curve was obtained from a TomoTherapy unit operated

Table 1 List of CT scanners used in this study and the manufacturers. The numbers in parenthesis are the number of CT scanners of the same model, but from different institutions

CT scanner model	Manufacturer
Philips Brilliance 16 (2)	Philips
Philips Brilliance	
Philips PET-CT TF TOF16	
Philips iCT 256	
Philips Bigbore	
GE Hi Speed (2)	GE
GE Light Speed (2)	
GE Light Speed 16	
Siemens Biograph 16	
Siemens Cardiac 64	Siemens
Siemens Plus 4	
Siemens Sensation Open 16	
Siemens Sensation Open 48	
Toshiba	Toshiba
Picker	Picker international
Tomotherapy (MVCT)	Accuray

in a scanner mode with 1 MV x rays for imagining as advocated by Lengen *et al.* (15). *Table 1* lists the CT scanners involved in this study and their respective manufacturers. A majority of the CT scanners (16/18) were from one of three vendors: Philips (Philips Healthcare, Andover, MA), GE, or Siemens (Siemens USA, Malvern, PA). The remaining two are from two separate vendors: Toshiba (Toshiba America Medical Systems, Inc., Tustin, CA) and Picker International (Picker International, Cleveland, OH).

Five RMI 467 phantoms were used to obtain the different TCC. There were two identical pairs of phantoms as they had identical RED data sheet. Thus practically, only three different RMI phantoms were used for the calibration of the CT scanners. They are labeled as RMI 1, RMI 2 and RMI 3 for identification purpose. Except for one RMI phantom (RMI 3), each of the remaining four phantoms (two under RMI 1 and two under RMI 2) were used for the calibration of more than one CT scanners. Additional inserts were used for RMI 1 to generate calibration points in the RED range between 0.936-1.137.

The RED was converted to RSP using the Bethe-Bloch formula [Eqn. 1] and ionization energies published in ICRU49 (16). The RSP values were calculated for 208 MeV proton energy, which is the maximum energy at our center. *Table 2* lists the tissue substitute materials

Table 2 A list of tissue substitute inserts in the RMI 467 tissue characterization phantom and the associated ranges of relative electron densities and relative stopping powers for the five phantoms

Tissue substitute material	Relative electron density	Relative stopping power
LN-300	0.283±0.014	0.282±0.014
LN-450	0.433±0.009	0.432±0.009
AP6	0.910±0.021	0.917±0.022
BR-12 breast	0.962±0.008	0.968±0.006
Solid water	0.990±0.002	0.991±0.001
Water	1.000	1.000
BRN-SR2 brain	1.041±0.010	1.054±0.012
LV1 liver	1.057±0.016	1.060±0.018
IB inner bone	1.087±0.014	1.074±0.016
B200 bone mineral	1.099±0.009	1.085±0.010
CB2-30%	1.276±0.003	1.260±0.005
CB2-50%	1.464±0.004	1.423±0.007
SB3-cortical bone	1.694±0.002	1.626±0.005
Polyethylene*	0.936	0.958
CB3 resin*	1.011	1.023
CB resin (CB4)*	1.106	1.109
CB2-10% CaCO ₃ *	1.132	1.132
Acrylic*	1.137	1.137

*additional inserts used by some of the CT scanners

used in the RMI phantoms, and their respective RED and RSP values averaged over the five phantoms ±1 SD. The tissue substitute materials marked with an asterisk are the additional inserts used by two institutions for their CT scanners. Since the RMI phantoms have identical RED for the tissue substitute materials, no average values and standard deviations were calculated for these additional inserts. *Table 2* shows that for the lowest density material the RED variation is about 5%. For RED between 0.4-0.99, the variation in RED values among the five phantoms is ≤2%. For RED>1, the density variation is ≤1%. For each tissue substitute material, the different HU obtained from the 18 scanners is separated into three groups based on their phantom number.

Since RSP of a material is derived from its corresponding RED value from a very complex equation [Eq. 1], it is interesting to compare the HU-RSP and its corresponding HU-RED curves. As an example, the two curves are compared for the Siemens Biograph 16 CT scanner used at the Proton Therapy Center.

Comparison of HU-RSP curves for the different CT scanners

In addition to the variation of the RED values (and hence RSP) for the tissue substitute materials among the three different RMI phantoms, the HU for a given tissue substitute material may vary from one CT scanner to another, even for the same tissue characterization phantom due mainly to the difference in the energy spectra of the X-rays. To examine the variation of the HU-RSP curves among the different CT scanners of the same vendor, the various HU-RSP curves were compared for the three vendors: Philips, GE and Siemens.

Using the same RMI phantom, the HU-RSP curves were obtained for nine CT scanners from various vendors to investigate the effect of the X-ray spectrum in the different CT scanners on the TCC.

Finally, to examine the extent of variation of the HU-RSP curves for all the scanners in the study, the 18 TCC were compared in the same graph. The portion in the TCC for some of the CT scanners which included the additional inserts was excluded from the curves so that all HU-RSP curves contained the same tissue substitute materials. The HU-RSP curve obtained from a TomoTherapy unit which is operated at 1 MV in the imaging mode is also included for comparison as well as to demonstrate the difference between tissue characterization between MVCT and kVCT. The difference is especially relevant in proton therapy for patients with metallic implants, as reported by Yang *et al.* (17).

Effect of differences in HU-RSP curves on dose distributions

In treatment planning of PBT, the RSP value associated with each pixel in a CT image is obtained from the HU-RSP curve. To study the effects of differences in the HU-RSP curves on dose distributions, instead of using all 18 HU-RSP curves in treatment planning, we elected to generate HU-RSP curves, which represent the minimum and maximum HU-RSP curves with respect to the HU axis for dose calculation. To this end, the minimum and maximum HU of each tissue substitute material and its corresponding average RSP value (RSP_{av}) are used to form two HU-RSP curves, $HU_{min}-RSP_{av}$ and $HU_{max}-RSP_{av}$ respectively, representing the largest change in the HU-RSP curves. In addition, a HU-RSP curve was formed by using the average HU of each material and the corresponding RSP_{av} , which is the average HU-RSP curve

for the 18 scanners. For each HU-RSP curve (min, max and mean), dose distributions were calculated for a prostate and a head and neck proton treatment plan, respectively. The DVH of the GTV, PTV and a number of organs at risks were then determined and compared with those obtained from the respective 'reference plan', which was generated by using the HU-RSP curve for the IUHPTC planning system currently in use clinically.

Results

Comparison of HU variation in different RMI phantoms

Figure 1 shows the HU variation across CT scanners for three tissue substitute materials (LN-300, water and cortical bone) within each RMI phantom as examples. The HU where the X-axis intersects with the Y-axis corresponds to the mean value of the HU. The numbers on the X-axis represent the phantom number (zero is the origin on the plot). For LN-300, larger HU variations are observed for RMI-1 compared to RMI-2 as shown in Figure 1A. The HU for RMI-3 is unusually high compared to all other points. For water, there is an unusually low HU for one institution in RMI-1. Otherwise, most of the remaining points (14/15) are within 1SD of each other. For cortical bone, the HU shows larger variation for RMI-1 compared to those from RMI-2.

Figure 2 compares a HU-RED curve and the corresponding HU-RSP curve for the Siemens Biograph 16 CT scanner. It can be seen that the two calibration curves track each other very closely in the region from lung to an RED (RSP) value of about 200. The curves start to separate from each other with RED slightly higher than the corresponding RSP value from about 1% at HU ~450 to about 4% at HU ~1200, corresponding to the cortical bone.

Comparison HU-RSP curves for the different CT scanners

Figure 3(A-C) compares the HU-RSP curves for the Siemens, GE and Philips CT scanners involved in the study respectively. The portion of the curves circled in Figure 3A (magnified in the inset) contains additional calibration points in the RSP range between 0.9-1.14. These points represent phantom materials (highlighted in Table 2) with higher percentage of carbon but no phosphorus or calcium compared to other materials of similar RSP which have about 9% calcium and 3% phosphorus. A similar structure in the HU-RSP curve is also shown for the GE Hi Speed

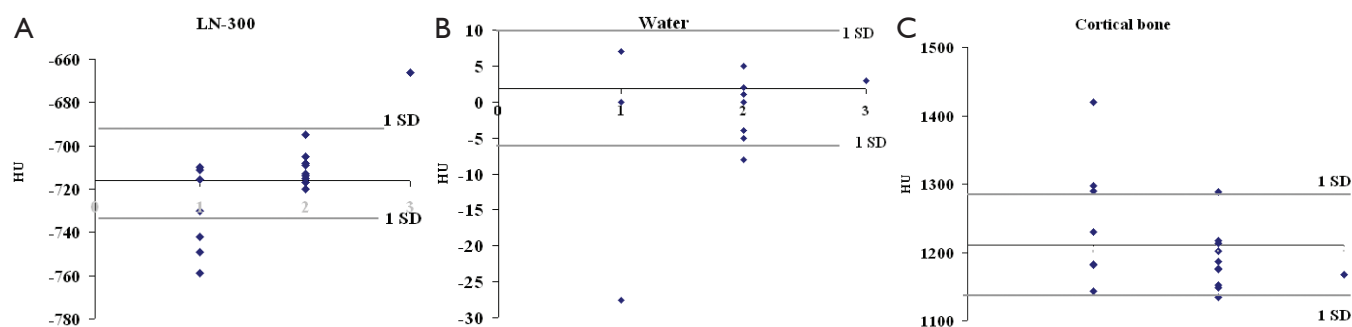


Figure 1 A. Variation of HU for the lung substitute material, LN-300, in the three RMI phantoms. The HU where the x-axis intercepts with the Y-axis is the mean HU, averaged over all 18 points. The numbers on the X-axis are the phantom numbers (the zero is the origin of the X-axis). Larger variation in HU can be observed for RMI 1, compared to those in RMI 2. HU for RMI 3 is much higher than the rest; B. Variation of HU for water in the three different RMI phantoms. The HU where the X-axis intercepts with the Y-axis is the mean HU. Note that most of the HU for water were within 1 SD of each other, except two institutions with unusually low HU; C. Variation of HU for the cortical bone in the three RMI phantoms. Again, the mean HU value is where the X-axis intersects with the Y-axis. The HU for the cortical bone show larger variation compared to those in RMI 2

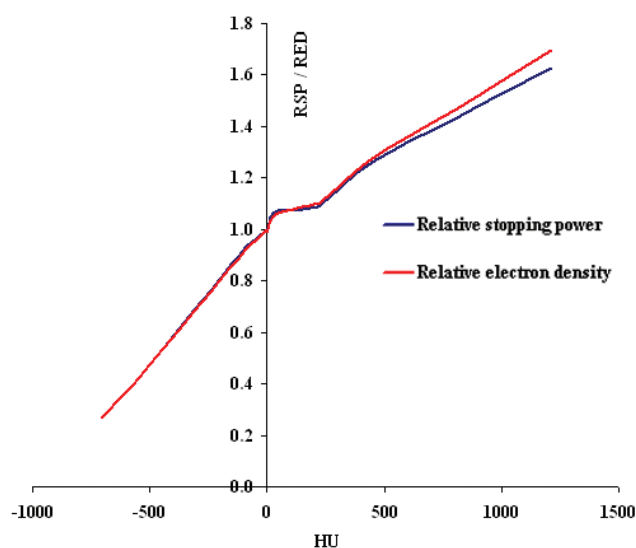


Figure 2 Comparison of HU-RED and the HU-RSP curves for the Siemens Biograph 16 CT scanner

1 in *Figure 3B* for the same reason. The presence of these points results in ambiguity in the calibration curve as a given HU in that region corresponds to more than one RSP values. The HU-RSP curves for the Philips CT scanners chosen for this study are remarkably similar as shown in *Figure 3C*.

Figure 4 compares the HU-RSP curves obtained for the same RMI phantom for nine different CT scanners. The curves look remarkably similar for all nine CT scanners in the region $-700 < \text{RSP} < 500$. Above $\text{RSP} = 500$, the curves

begin to show some separations. However, when examining closely, the largest separation occurs at $\text{RSP} \sim 1.633$ with 1 SD of the variations at about 3%. On the other hand, the SD of the HU variation is about 30% for the SR2 brain insert corresponding to $\text{RSP} = 1.062$. The large % difference is probably due to the small HU for the brain substitute materials, in the range 8-24.

To remove the ambiguity in the HU-RSP curves as shown in the inset of *Figure 3A*, these additional points were removed from the respective calibration curves and re-plotted in *Figure 5* together with all other curves to investigate the extent of variation among the 18 HU-RSP curves. The curves generally can be represented by three straight lines in the three HU intervals: $-700 < \text{HU} < 0$, $0 < \text{HU} < 230$ and $230 < \text{HU} < 1,700$.

In the HU range -700 to zero, the HU-RSP curves are roughly parallel to each other. For a given RSP, the variation in HU among the 18 CT scanners is within about 10%. The region immediately above water ($\text{RSP} = 0$) to $\text{RSP} \sim 1.1$ is almost horizontal resulting in a large variation in HU for a small change in RSP. The HU changes from about 5 to 300 for $\text{RSP} = 1$ to 1.1 (water to bone mineral region). In the RSP region corresponding to the liver substitute ($\text{RSP} \sim 1.05$ - 1.07), the HU changes from a minimum of 58 to 106, depending on the model and manufacturer of the CT scanners. The mean HU value, HU_{mean} for liver was 84.3 ± 8.30 . In the bone region, corresponding to $\text{RSP} > 1.1$, the curves start to separate from each other. For the CB2-30% substitute, the HU changes from a minimum of 407 to a maximum of 539. The HU_{mean} is 447 ± 34.0 . For the

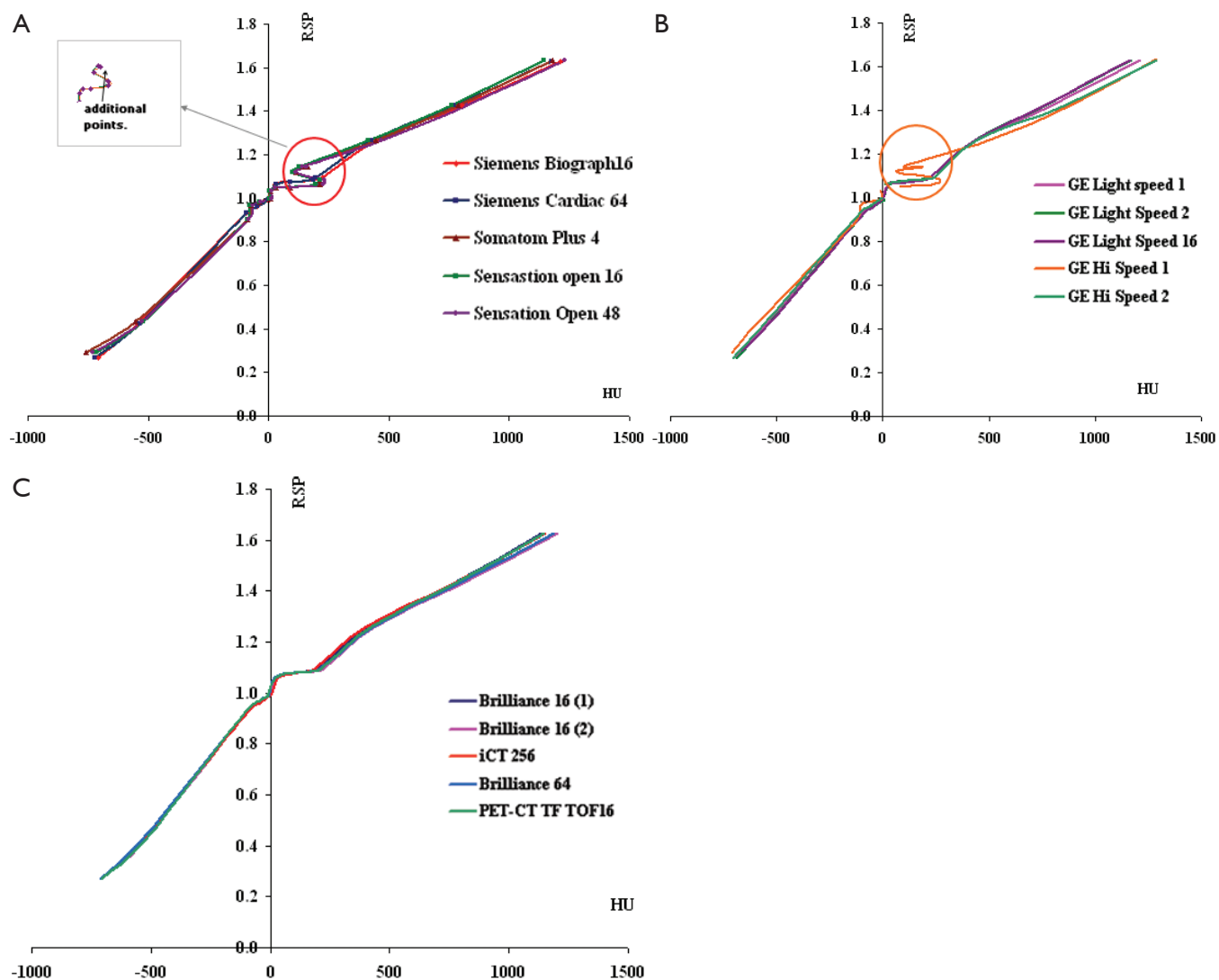


Figure 3 A. Comparison of HU-RSP curves for the different Siemens CT scanners. The region inside the circle is magnified to show the behavior of the curves due to additional inserts used to obtain the curves for some of the CT scanners; B. Comparison of HU-RSP curves for the different GE CT scanners. The strange behavior of the region inside the circle for the GE Hi Speed 1 CT scanner is due to additional inserts used to obtain the curve; C. Comparison of HU-RSP curves for the different Philips CT scanners

cortical bone which is the highest RSP point, the HU changes from 1,140 to 1,420 with a mean value of $1,210 \pm 720$ (1 SD).

Two HU-RSP curves for a particular institution were distinctively different from the rest of the group (the GE Hi Speed 1 in *Figure 3B* is one of the two, the other curve is the Toshiba Aquilion scanner). If these two curves are removed, the HU-RSP curves for this group of remaining 16 CT scanners show smaller deviations from each other, especially in the RSP region >1.1 as shown in *Figure 6*. For example, for the CB2 bone, the $HU_{min}=407$,

and the $HU_{max}=490$, with the $HU_{mean}=438 \pm 21.1$. For the cortical bone, $HU_{min}=1,140$, $HU_{max}=1,300$, with the $HU_{mean}=1,190 \pm 47.3$. The variations of HU with respect to RSP were then described by the two HU-RSP curves representing the minimum and maximum of the HU for a given RSP.

It is interesting to note that for the TomoTherapy unit, the HU-RSP curve is almost linear for the entire range of HU. This is due to the fact that the attenuation of MeV photons is predominantly due to Compton interaction, which has a weak dependence on Z.

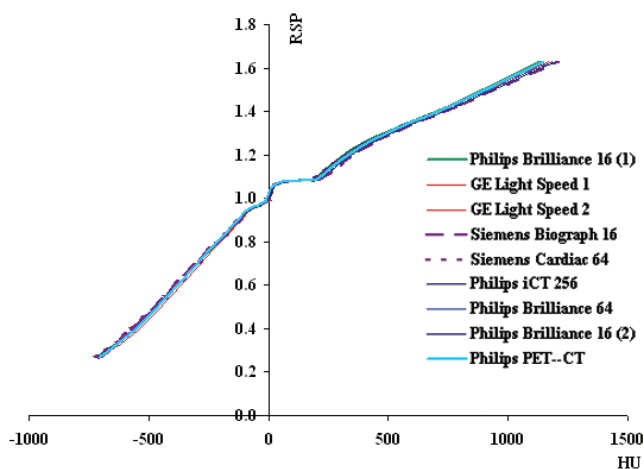


Figure 4 Comparison of HU-RSP curves for nine CT scanners obtained with the same RMI 467 phantom

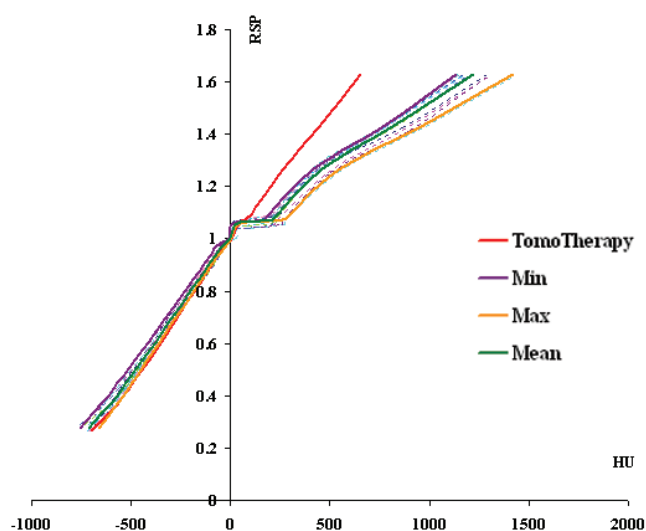


Figure 5 HU-RSP curves for all 18 CT scanners (dashed lines). The characterization curve obtained from a TomoTherapy unit is included for comparison. Also included are the three HU-RSP curves: HU_{\min} -RSP_{av}, HU_{\max} -RSP_{av} and HU_{mean} -RSP_{av}, labeled as min, max and mean in the graph

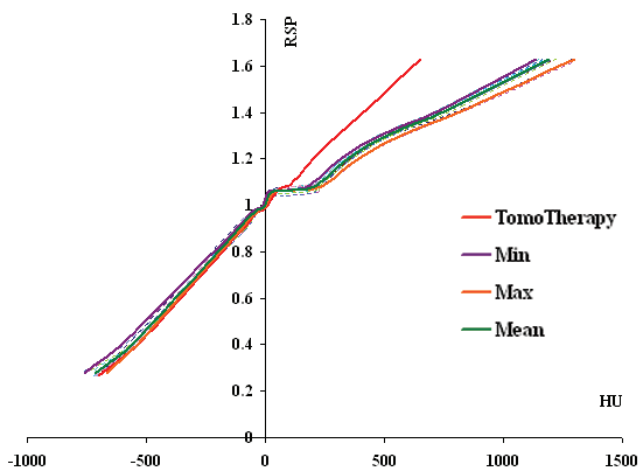


Figure 6 After removing the two HU-RSP curves from one institution which both showed distinctly different behavior from the other curves, the remaining 16 HU-RSP curves are plotted. A new set of HU_{\min} -RSP_{av}, HU_{\max} -RSP_{av} and HU_{mean} -RSP_{av} curves were obtained

Effect of differences in HU-RSP curves on dose distributions

Table 3 compares the minimum, maximum and mean doses from the DVHs of the volumes of interest (GTV, PTV1, PTV2, bladder, rectum and seminal vesicle) for a prostate case. Since an opposed lateral beam configuration is used in the treatment, the major inhomogeneities involved are the femoral heads and the rectal balloon which is filled with a contrast medium of RSP=1.2. The HU-RSP curves (min, max, mean) used in the calculation were obtained without

the two distinctly different HU-RSP curves. It can be seen that the three HU-RSP curves (min, max, mean) produce very similar DVH parameters for the volumes of interest when compared with those obtained from the clinical HU-RSP curve (labeled as IUHPTC120). Indeed, the min, max and mean doses for all the volumes of interest were within 1% for all but the minimum dose to the PTV1, which was about 4.5% smaller than that from IUHPTC120.

Table 4 compares the minimum, maximum and mean doses from the DVHs of the volumes of interest for a head and neck case. Due to the complex shape of the target volumes, complicated beam setup was used. Despite the presence of inhomogeneities such as air cavities and bone, all three HU-RSP curves (min, max, mean) yielded DVH results for the various volumes of interests to within 5% of those obtained with the clinical calibration curve for the majority of the dose parameters examined. However, deviations >10% from the IUHPTC120-based plan in the dose parameters were observed for the optic nerves and cochlea for both the HU_{\min} -RSP and HU_{\max} -RSP plans. The DVHs for the HU_{mean} -RSP plan, on the other hand, agreed with the OIHPTC120 plan to within 4%.

Discussion and conclusions

We have compared the HU-RSP curves for 18 CT scanners

Table 3 Comparison of the min, max and mean doses for the different volumes of interest in a prostate plan in proton therapy

Prostate		Min dose	Max dose	Mean dose
PTV1	HU-RSP-MIN	4,627	8,168	7,333
	HU-RSP-MAX	4,839	8,132	7,348
	HU-RSP-MEAN	4,833	8,149	7,349
	IUHPRC120	4,834	8,153	7,348
PTV2	HU-RSP-MIN	5,982	8,168	7,898
	HU-RSP-MAX	5,966	8,132	7,875
	HU-RSP-MEAN	5,973	8,149	7,887
	IUHPRC120	5,970	8,153	7,888
GTV	HU-RSP-MIN	7,675	8,164	7,926
	HU-RSP-MAX	7,673	8,118	7,893
	HU-RSP-MEAN	7,679	8,137	7,908
	IUHPRC120	7,677	8,145	7,909
Bladder	HU-RSP-MIN	0	8,061	897
	HU-RSP-MAX	0	8,031	943
	HU-RSP-MEAN	0	8,045	924
	IUHPRC120	0	8,048	923
Rectum	HU-RSP-MIN	0	7,339	2,138
	HU-RSP-MAX	0	7,344	2,128
	HU-RSP-MEAN	0	7,341	2,133
	IUHPRC120	0	7,340	2,133
Seminal vesicle	HU-RSP-MIN	5,070	8,000	6,606
	HU-RSP-MAX	5,056	7,962	6,593
	HU-RSP-MEAN	5,069	7,980	6,601
	IUHPRC120	5,067	7,982	6,602

and a TomoTherapy unit operated in the imaging mode. The CT scanners were from five different manufacturers. Five RMI 467 phantoms, two of which were an identical pair, were used to generate the HU-RSP curves. Thus practically, only three different RMI phantoms were used for the 18 HU-RSP curves. Here, we assumed that the elemental compositions of the tissue substitutes were identical so long as their RED values were the same. There was a small variation (<2%) in RED (and RSP) among the three different RMI phantoms for all tissue substitute materials except for LN-300, which had about 5% variation among the three phantoms.

The variations of the HU within each RMI phantom group generally show larger variation for RMI 1 as shown by the three representative materials in *Figure 1*. If we assume that phantoms within the same group were truly identical, the variation in HU indicates the source of variation being the different x ray spectra of the different

CT scanners.

Figure 3A-C shows that even for CT scanners from the same vendor, the HU-RSP curves may deviate from each other. There are two factors that may contribute to the HU variation: the difference in the x ray spectra of the CT scanners and the variation in the chemical composition of the 'same' tissue substitute materials in the different RMI phantoms. The minimum HU was in general 7-10% lower than the maximum HU, for all tissue substitute materials and for all CT scanners in the study.

On the other hand, using the same RMI phantom the HU-RSP curves for nine CT scanners from various vendors are remarkably similar as shown in *Figure 4*. For cortical bone, the minimum HU was about 5% smaller than the maximum HU. For LN-300, the minimum HU was about 2.5% smaller than the maximum HU. The results seem to indicate that the chemical compositions of the tissue substitute materials have a larger effect on the HU than the

Table 4 Comparison of the min, max and mean doses for the different volumes of interest in a head and neck plan in proton therapy

H&N		Min dose	Max dose	Mean dose	H&N	Min dose	Max dose	Mean dose
PTV	HU-RSP-MIN	4,512	6,370	5,768	R optic nerve	0	3,812	1,152
	HU-RSP-MAX	4,925	6,366	5,761		5	3,996	1,592
	HU-RSP-MEAN	4,753	6,367	5,765		2	3,890	1,391
	IUHPRC120	4,712	6,368	5,767		1	3,866	1,305
CTV	HU-RSP-MIN	5,033	6,368	5,781	Brainstem	5,264	5,950	4,622
	HU-RSP-MAX	5,039	6,366	5,771		5,250	5,960	5,612
	HU-RSP-MEAN	5,048	6,367	5,776		5,257	5,956	5,617
	IUHPRC120	5,050	6,366	5,779		5,260	5,954	5,619
GTV	HU-RSP-MIN	5,054	6,300	5,758	Cord	0	5,406	2,715
	HU-RSP-MAX	5,039	6,294	5,747		0	5,397	2,710
	HU-RSP-MEAN	5,048	6,297	5,752		0	5,402	2,713
	IUHPRC120	5,050	6,299	5,754		0	5,403	2,713
Optic chiasm	HU-RSP-MIN	3,638	5,020	4,152	L cochlea	3,559	5,969	5,229
	HU-RSP-MAX	3,667	5,370	4,506		4,904	6,045	5,736
	HU-RSP-MEAN	3,656	5,217	4,312		4,304	6,024	5,545
	IUHPRC120	3,651	5,158	4,278		3,754	5,994	5,341
L optic nerve	HU-RSP-MIN	0	3,750	1,028	R Cochlea	855	4,485	2,695
	HU-RSP-MAX	0	3,985	1,278		880	4,618	2,807
	HU-RSP-MEAN	0	3,852	1,164		862	4,553	2,747
	IUHPRC120	0	3,823	1,127		855	4,508	2,712

X-ray spectrum.

The calibration curves for all CT scanners generally exhibit similar shapes and can be described by three linear segments in three distinct HU regions: $[-700, 0]$, $[0, 1,100]$ and $[1,100, 1,700]$. The largest deviations in the HU-RSP curves among the different CT scanners occur in the bone region where $RSP > 1.4$. The 18 HU-RSP curves showed substantial variation over the range of HU from -700 to $1,700$. However, by removing the two curves from one institution, which seem to have distinctly different behavior, the variations of the HU-RSP curves for the remaining 16 scanners were substantially reduced. The HU_{min} - RSP_{av} and HU_{max} - RSP_{av} curves followed closely the envelop of the 16 curves.

Despite the relatively large variation of between the HU_{min} - RSP_{av} and HU_{max} - RSP_{av} curves, the minimum, maximum and mean doses from the DVHs of the volumes of interests for a prostate plan obtained with these two calibration curves were within 1% of those obtained with the clinical calibration curve and the HU_{mean} - RSP_{av} curve, which represent the average HU-RSP curve of all 16 CT scanners. For the head-and-neck plan, the agreement was still within 5% for most dose points for the various volumes

of interests. Our results indicate that 7-10% differences between the HU-RSP curves had $<5\%$ effect even in a complex head and neck plan with the presence of several inhomogeneities.

This study did not address the issue of metallic implants as this was beyond the scope of this work. Rather it shows that while both elemental compositions of the tissue substitutes and the variation in the X-ray spectrum among the CT scanners contribute to the HU variation for a given RSP value, the effect of the X-ray spectrum, and hence the beam hardening effect is smaller than that due to difference in elemental compositions. This is in agreement with the study by Qi *et al.* (14). On the other hand, despite the large variation among the HU-RSP (min, max and mean) curves, the minimum, maximum and the mean doses for the target volume as well as for the OAR were generally in very good agreement with the reference plan. The excellent agreement between the dose calculation results using HU_{mean} - RSP_{av} and those from the clinical HU-RSP curve seems to suggest that a single HU-RSP reference curve, generated by a large number of treatment planning CT scanners, may be used for proton therapy. A similar conclusion has been reported for 6 MV

X-rays by Thomas (5).

This study does not recommend the use of a single HU-RSP curve without a CT calibration. On the contrary, a user has to do a calibration of his/her own scanner using a tissue characterization phantom and then compare the curve with the 'universal' curve to decide if the latter is suitable to be used. This is similar to the golden data offered by linac vendors. Indeed, a golden beam data has also been recently proposed for proton pencil beams used in active beam scanning (18). A clinic which purchases the golden data for a linac still has to obtain a number of beam scanning data to verify that the golden data is suitable for their clinic. Thereafter, beam data would still need to be scanned annually to confirm the suitability and stability of the beam so that the golden data could be used. A HU-RSP reference curve may be used in a similar manner.

In summary, the present work is the first study that examined a large number (18) of kVCT scanners that are newer models commonly used in the clinic. In addition, a MVCT was also studied. Further, our study is also the first to look at the differences in dose distributions in proton therapy due to variations in HU-RSP curves. Our study showed that the differences in HU-RSP curves obtained from tissue substitute materials appear to affect the minimum, maximum and mean dose parameters of a representative prostate treatment plan by less than 1% and that of a representative head and neck plan by less than 4%. This suggests the usefulness of a single 'averaged' HU-RSP reference curve.

Acknowledgments

This paper was partially presented as a poster in the AAPM annual meeting in 2010.

Funding: None.

Footnote

Provenance and Peer Review: This article was commissioned by the Guest Editors (Huan Giap and Eric Y Chuang) for the series "Particle Beam Therapy II" published in *Translational Cancer Research*. The article has undergone external peer review.

Conflicts of Interest: All authors have completed the ICMJE uniform disclosure form (available at <http://dx.doi.org/10.3978/j.issn.2218-676X.2012.11.05>). None of the

authors has any financial interests with any of the CT vendors.

Ethical Statement: The authors are accountable for all aspects of the work in ensuring that questions related to the accuracy or integrity of any part of the work are appropriately investigated and resolved.

Open Access Statement: This is an Open Access article distributed in accordance with the Creative Commons Attribution-NonCommercial-NoDerivs 4.0 International License (CC BY-NC-ND 4.0), which permits the non-commercial replication and distribution of the article with the strict proviso that no changes or edits are made and the original work is properly cited (including links to both the formal publication through the relevant DOI and the license). See: <https://creativecommons.org/licenses/by-nc-nd/4.0/>.

References

1. Levi C, Gray JE, McCullough EC, et al. The unreliability of CT numbers as absolute values. *AJR Am J Roentgenol* 1982;139:443-7.
2. Faulkner K, Moores BM. Variations in measured computed tomography number values. *Radiography* 1985;51:163-7.
3. Constantinou C, Harrington JC, DeWerd LA. An electron density calibration phantom for CT-based treatment planning computers. *Med Phys* 1992;19:325-7.
4. Coolens C, Childs PJ. Calibration of CT Hounsfield units for radiotherapy treatment planning of patients with metallic hip prostheses: the use of the extended CT-scale. *Phys Med Biol* 2003;48:1591-603.
5. Cozzi L, Fogliata A, Buffa F, et al. Dosimetric impact of computed tomography calibration on a commercial treatment planning system for external radiation therapy. *Radiother Oncol* 1998;48:335-8.
6. Kilby W, Sage J, Rabett V. Tolerance levels for quality assurance of electron density values generated from CT in radiotherapy treatment planning. *Phys Med Biol* 2002;47:1485-92.
7. Thomas SJ. Relative electron density calibration of CT scanners for radiotherapy treatment planning. *Br J Radiol* 1999;72:781-6.
8. Schneider U, Pedroni E, Lomax A. The calibration of CT Hounsfield units for radiotherapy treatment planning. *Phys Med Biol* 1996;41:111-24.
9. Bichsel H. eds. Passage of charged particles through matter, In American Institute of Physics Handbook. New

- York: McGraw-Hill, 1972.
10. Yohannes I, Kolditz D, Kalender WA. Semiempirical analysis of materials' elemental composition to formulate tissue-equivalent materials: a preliminary study. *Phys Med Biol* 2011;56:2963-77.
 11. Yohannes I, Kolditz D, Langner O, et al. A formulation of tissue- and water-equivalent materials using the stoichiometric analysis method for CT-number calibration in radiotherapy treatment planning. *Phys Med Biol* 2012;57:1173-90.
 12. ICRU Report 44. Tissue substitutes in radiation dosimetry and measurement. In. Bethesda, MD: International Commission on Radiation Units and Measurements, 1989.
 13. Schaffner B, Pedroni E. The precision of proton range calculations in proton radiotherapy treatment planning: experimental verification of the relation between CT-HU and proton stopping power. *Phys Med Biol* 1998;43:1579-92.
 14. Qi ZY, Huang SM, Deng XW. Calibration of CT values used for radiation treatment planning and its impact factors. *Ai Zheng* 2006;25:110-4.
 15. Langen KM, Meeks SL, Poole DO, et al. The use of megavoltage CT (MVCT) images for dose recomputations. *Phys Med Biol* 2005;50:4259-76.
 16. ICRU Report 49. Stopping Powers and Ranges for Protons and Alpha Particles. In. Bethesda, MD: International Commission on Radiation Units and Measurements, 1993.
 17. Yang M, Virshup G, Mohan R, et al. Improving accuracy of electron density measurement in the presence of metallic implants using orthovoltage computed tomography. *Med Phys* 2008;35:1932-41.
 18. Clasié B, Depauw N, Fransen M, et al. Golden beam data for proton pencil-beam scanning. *Phys Med Biol* 2012;57:1147-58.

Cite this article as: Cheng CW, Zhao L, Wolanski M, Zhao Q, James J, Dikeman K, Mills M, Li M, Srivastava SP, Lu XQ, Das IJ. Comparison of tissue characterization curves for different CT scanners: implication in proton therapy treatment planning. *Transl Cancer Res* 2012;1(4):236-246. doi: 10.3978/j.issn.2218-676X.2012.11.05